X-RAY PHOTOELECTRON SPECTROSCOPY AND RAMAN STUDIES OF ZnO:Ce NANOCRYSTALS [1]

G. Achamma [1*], M. S. Qureshi [2], M. M. Malik [2]

[1] Catholicate College, Pathanamthitta Kerala, India; e-mail: gachamma@gmail.com
[2] Maulana Azad National Institute of Technology, Bhopal, India

Cerium-doped ZnO nanopowders were synthesized using the simple refluxing technique. The synthesized samples were characterized by X-Ray diffraction, which confirmed their hexagonal structure. No additional peaks due to the interstitial incorporation or substitutions of Ce^{4+} ions into the ZnO lattice were observed. Ce $3d_{3/2}$ and $3d_{5/2}$ had well-separated orbits of Δ = 18.26 eV. The observed spin-orbit splitting as well as the separation between $3d_{5/2}$ peaks by 16.47 eV were in good agreement with those reported. The presence of 917.85 eV also confirmed the presence of Ce^{4+} ions. Raman studies showed that for Ce-doped ZnO the nonpolar interaction E_{2H} grew strong and had a dominant intensity.

Keywords: *nanocrystal, nanopowder, X-Ray diffraction, Raman spectroscopy.*

ИССЛЕДОВАНИЕ НАНОКРИСТАЛЛОВ ZnO:Ce МЕТОДАМИ РЕНТГЕНОВСКОЙ ФОТОЭЛЕКТРОННОЙ СПЕКТРОСКОПИИ И КОМБИНАЦИОННОГО РАССЕЯНИЯ СВЕТА

G. Achamma [1*], M. S. Qureshi [2], M. M. Malik [2]

УДК 535.375.5;620.3

[1] Католический колледж, Патанамитта Керала, Индия; e-mail: gachamma@gmail.com
[2] Национальный институт технологии Маулана Азада, Бхопал, Индия

(Поступила 8 августа 2018)

Нанопорошки ZnO, легированные церием, синтезированы простым методом кипячения с обратным холодильником. Синтезированные образцы охарактеризованы с помощью рентгеновской дифракции, которая подтверждает гексагональную структуру; из-за междоузельного взаимодействия или замещения ионов Ce^{4+} в решетке ZnO никаких дополнительных пиков не наблюдалось. Ce $3d_{3/2}$ и $3d_{5/2}$ имеют хорошо разделенные орбиты Δ = 18.26 эВ. Наблюдаемое спин-орбитальное расщепление, как и разделение пиков $3d_{5/2}$ на 16.47 эВ, согласуется с известными данными. Наличие пика, соответствующего 917.85 эВ, подтверждает существование в веществе ионов Ce^{4+}. Исследования методом спектроскопии комбинационного рассеяния света показывают, что для ZnO, допированного ионами церия, неполярное взаимодействие E_{2H} становится сильным и доминирует.

Ключевые слова: *нанокристалл, нанопорошок, метод рентгеновской дифракции, спектроскопия комбинационного рассеяния света.*

Introduction. Cerium, being the first member of the lanthanide series, can possess anomalous emission characteristics (from the UV to the red region). It is chosen as a suitable dopant for ZnO, which has numerous defect states [1]. Cerium oxide, being one of the superantioxidants and a form of the rare earth metal cerium, remains relatively stable as it cycles between cerium oxide III and IV. In the first state, nanoparticles have gaps in their surface that absorb oxygen ions like a sponge. When cerium oxide III is mixed with free radicals, it catalyzes a reaction that effectively defangs the reactive oxygen species (ROS) by capturing oxygen atoms and turning them into cerium oxide IV. Cerium oxide IV particles slowly release their captured

[1] Presented at ICMS conference MG University, Kottayam, Kerala.

oxygen and revert to cerium oxide III, so they can break down free radicals again and again. Cerium can help treat traumatic brain injury, cardiac arrest, and Alzheimer's patients, guard against radiation-induced side effects suffered by cancer patients, and perhaps even slow the effects of aging [2]. Several authors have reported ZnO:Ce as a photo-catalytic and antioxidant agent [2–7].

We have reported the synthesis and detailed diffraction studies of ZnO:Ce [8]. Previously, the influence of Ce^{3+} was anticipated, but here we are able to confirm the presence of Ce^{4+} ions in the ZnO lattice. As there are many luminescence properties of defects in doped ZnO [1, 7], we have extended our earlier work by characterization with Raman and X-ray spectroscopies.

Experimental. GR grade (purity> 99%) zinc acetate ($Zn(CH_3COO)_2 \cdot 2H_2O$), cerium nitrate ($Ce(NO_3)_3 \cdot 6H_2O$), urea ($CH_2NH_2COOH$), and ethylene glycol ($C_2H_6O_2$) were procured from E. Merck India. No further purification was carried out. In a typical experiment, 0.5 g of zinc acetate was dissolved in 50 mL of ethylene glycol. Around 1.5 g of urea was added into this solution, and the temperature was raised up to 150°C and maintained at this value for 2 h. A white precipitate of ZnO was obtained, separated by centrifugation, and washed several times with quadruple distilled water and methanol (so as to remove traces of impurities). After that, the samples were dried at room temperature. For Ce (2 and 10 mol.%)-doped ZnO nanocrystals, the same procedure was followed; an appropriate amount of cerium nitrate was dissolved in the solution at the beginning of the reaction process.

The phase identification of the synthesized ZnO nanocrystals was performed on a Rigaku MiniFlex II with a CuK_α target (λ = 1.54060 Å) at room temperature. The X-ray generator was operated at 30 kV with a scan speed of 2°/min. An X-ray photoelectron spectroscopy (XPS) PHI Model 550 ESCA/SAM system 600 W was used to study the XPS spectra. A micro Raman system Jobin Yvon Horiba LABRAM-HR Visible (400–1100 nm) was used for Raman measurements.

Results and discussion. To ascertain the crystalline nature of pristine and doped ZnO nanocrystalline powders, X-Ray diffraction studies were performed. The pattern is shown in Fig. 1. The peaks located at 2θ values are ascribed as the (100), (002), (101), (102), (110), (103), (200), (112), and (201) crystal planes of wurtzite ZnO (JCPDS No 36-1451). In all the cases, the synthesized nanopowders are phase pure, and no additional signatures were observed. In the doped nanopowders, the presence of Ce^{4+} forming CeO_2 would have a peak at 2θ = 28.3° (JCPDS No 34-0394)), but here, due to the Ce^{4+} substitution or interstitial incorporation at the Zn^{2+} sites, no such peak was observed. In the present case, the broadening peak is assigned to the smaller crystallite size. From the 2θ values, the interplanar spacing d of the peaks is calculated (Table 1). The lattice parameters *a* and *c* increase slightly as the radii of Ce^{4+} (0.092 nm) are larger than those of Zn^{2+} (0.084 nm) (Table 2) we anticipate that at low Ce concentrations, interstitial incorporation is favored, while at high Ce concentrations, substitution and interstitial substitution are comparable processes [8, 9].

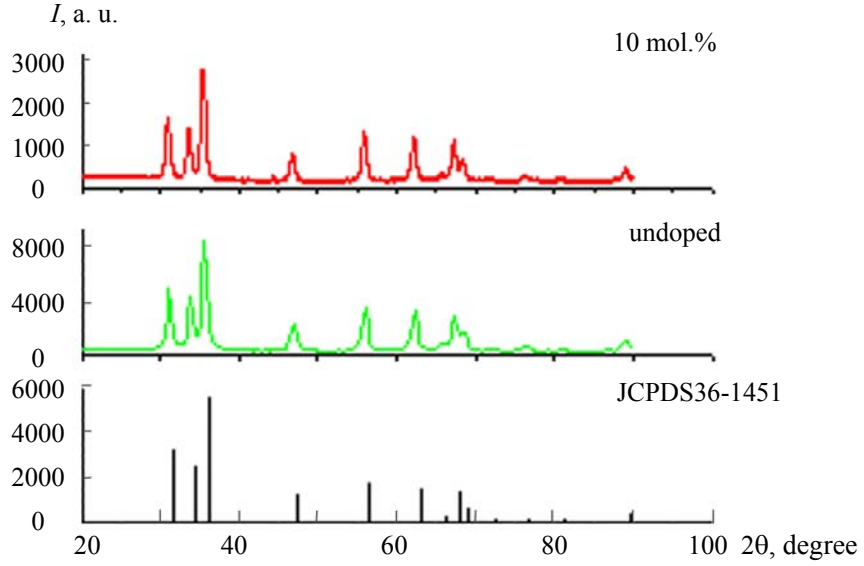

Fig. 1. X-ray diffraction pattern for undoped and Ce doped ZnO nanopowders and the standard data from JCPDS file No. 36-1451. No variation in peak positions is observed except for a few variations in intensities.

TABLE 1. Comparison of Observed and Calculated *d* values (Å) of Some Reflections of ZnO:Ce Nanopowders

h	*k*	*l*	$d_{undoped}$	$d_{cal\ 2mol.\%}$	$d_{cal\ 10mol.\%}$
1	0	0	2.865	2.910	2.920
0	0	2	2.649	2.664	2.664
1	0	1	2.529	2.533	2.529
1	0	2	1.934	1.941	1.934
1	1	0	1.641	1.649	1.647
1	0	3	1.489	1.496	1.489
2	0	0	1.419	1.423	1.419
1	1	2	1.387	1.392	1.392
2	0	1	1.365	1.373	1.374

TABLE 2. Variation of Lattice Parameters For Various Dopant Ion Concentrations

Ce, mol.%	*a*	*c*	*c/a*
0	3.25	5.22	1.6061
2.0	3.27	5.28	1.6146
10.0	3.28	5.29	1.6128

The formation of vibrational states due to Ce incorporation into the ZnO lattice is detected by the XPS studies for 10 mol.% doping. Here, in all the XPS spectra, the binding energies were calibrated by taking the carbon C 1*s* peak 284.6 eV as the reference. The high-resolution scans of O 1*s*, Zn 2*p*, Zn 3*d*, and Ce 3*d* are shown in Fig. 2 for 10 mol.%. In the O 1*s* region, the energy is 530.87 eV. The peaks located at 1023.18 and 1046.21 eV are associated with Zn $2p_{3/2}$ and Zn $2p_{1/2}$, respectively. The high resolution scans also show that the binding energy of Ce $3d_{5/2}$ located at 882.63 eV is of Ce(IV) and the energies of 899.59 eV and 917.85 eV are also of Ce(IV) (as also reported in [3, 4, 6]). This clearly indicates the presence of Ce^{4+}ions. Ce $3d_{3/2}$ and $3d_{5/2}$ have well-separated orbits of Δ = 18.26 eV the observed spin-orbit splitting is in good agreement with those reported. Meanwhile, the separation between $3d_{5/2}$ peaks is 16.47 eV [3, 8]. The multiplet peaks of Ce 3*d* may be due to the removal of the 3*d* core electron, and the 4*f* level is pulled down due to the core hole potential, causing the charge transfer from oxygen 2*p* to Ce 4*f* [3]. Figure 2 shows the peak at 9.55 eV, which is of Zn 3*d*.

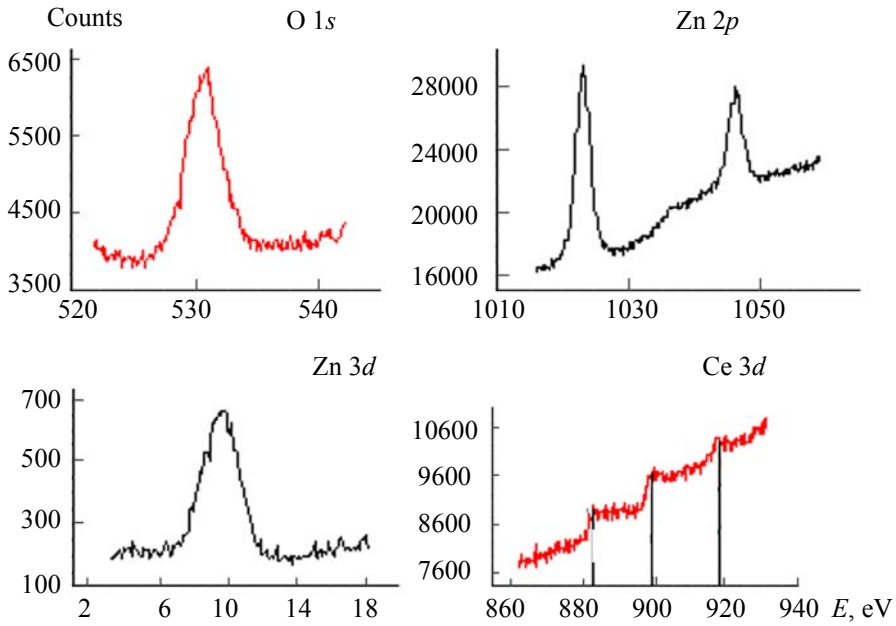

Fig. 2. XPS Spectrum of the Ce 10 mol.% doped ZnO sample annealed at 500°C

Raman scattering is very sensitive to the microstructure of nanosized materials. It is a nondestructive characterization method for studying the vibrational properties of ZnO nanostructures. Raman scattering is used here to clarify the quality and structure of ZnO nanocrystals. The wurtzite ZnO belongs to the space group C_{6v}^4 with two formula units in the primitive cell. Each primitive cell of ZnO has four atoms, each occupying C_{3v} sites, leading to 12 phonon branches, 9 optical modes, and 3 acoustic modes [9]. The optical phonons at the Γ point of the Brillouin zone belong to the following irreducible representation: $\Gamma_{opt} = 1A_1 + 2B_1 + 1E_1 + 2E_2$ [10]. For the optical modes, B_1 modes are Raman silent modes. For the long-range electrostatic forces, both A_1 and E_1 modes are polar and both Raman and infrared active, which split into transverse optical (TO) and longitudinal optical (LO) phonons. A nonpolar phonon mode with symmetry E_2 has two frequencies; E_{2H} is associated with oxygen atoms, and E_{2L} is associated with the Zn sublattice. Among the optical modes, A_1, E_1, and E_2 are Raman active [11]. The Raman spectra of the undoped and Ce-doped ZnO nanocrystals excited by the 488 nm line of an argon laser are shown (Fig. 3). The peaks located at 330.2, 380.8, 437.6, and 579.6 cm^{-1} are observed. The peaks located at 330.2, 380.8, and 437.6 cm^{-1} can be assigned to the second-order Raman spectra $2E_2$ (M), A_1, and E_{2H}, respectively. The strongest peak centered near 437.6 cm^{-1} is the characteristic mode (E_{2H}) for the hexagonal phase of ZnO. This nonpolar mode can be observed in the Raman spectra of all samples. It indicates the good crystallization of the nanocrystals and further confirms the results from XRD patterns. In addition, a broad peak located at 579.6 cm^{-1} can also be observed.

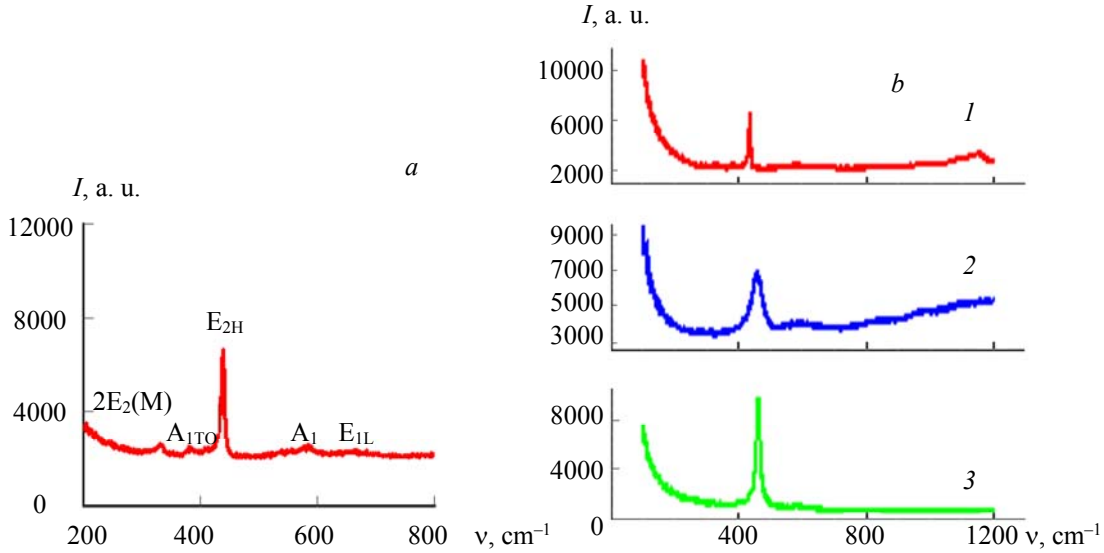

Fig. 3. Raman spectra for undoped ZnO (a) and comparative Raman spectra for undoped (1), 2 (2) and 10 mol.% (3) ZnO (b).

Usually, the peak located at 574 cm^{-1} in bulk ZnO corresponded to the A_{1L} phonon. It can be observed only in the configuration when the c-axis of wurtzite ZnO is parallel to the sample interface. When the c-axis is perpendicular to the sample interface, the E_{1L} (591 cm^{-1}) phonon is observed instead. According to the theory of polar optical phonons in wurtzite nanocrystals, the frequency of the 1LO phonon mode in ZnO should be between 574 and 591 cm^{-1}. So the peak near 579.6 cm^{-1} is due to the superimposition of A_{1L} and E_{1L} [11].

It should be noted that, for transition metal oxides, the Raman spectra reported in the literature vary from sample to sample depending on the size and morphology of the crystallites. It acquires a special significance for nanocrystals. The more affected bands are TO and LO and their splitting. The shifting of the Raman bands to higher wave numbers is due to the nanocrystalline nature. The weight of the Zn atom (65.39 a.m.u.) is about four times higher than that of the oxygen atom (15.99 a.m.u.). Hence, in the wurtzite structure of ZnO, vibrations from the oxygen atom are assumed to be involved. The E_{2H} mode is due to the nonpolar phonon mode. In Ce-doped ZnO this nonpolar interaction becomes strong, and the peak related to this interaction is shifted to 460 and 464 cm^{-1}. Here no signal is observed at 457 cm^{-1}, showing the presence

of CeO_2 originating from the Raman active mode characteristic of CeO_2, as the ZnO vibration is stronger than that of CeO_2. Similar results have been reported in [4, 12]. Suppression in the intensity of 330.2 and 380.8 cm^{-1} is observed. The A_1 (TO) mode shows the strength of the polar lattices bond. The decrease in the intensity supports the fact that the polar character of the wurtzite structure of ZnO is reduced when cerium ions are introduced.

The peak near 579.6 cm^{-1} is shifted to 605 cm^{-1}. This can also be considered as being due to the formation of defects such as oxygen vacancy and interstitial Zn [12]. The higher wavelength bands are assigned to either emission from the Ce lowest band (E_g) or to the formation of some new type of defects upon synthesis.

Conclusion. Ce-doped ZnO nanocrystals were synthesized using the reflux method. XPS and Raman studies were carried out to find the presence of Ce^{3+} or Ce^{4+} states. The presence of Ce $^{4+}$ ions was confirmed by XPS studies. We observed the binding energy of Ce 3*d* ($3d_{5/2}$ peaks) located at 882.63 and 899.53 eV with well-separated orbits of $\Delta = 16.47$ eV. Also 899.59 and 917.85 eV ($3d_{5/2}$ and $3d_{3/2}$) peaks had a separation of $\Delta = 18.26$ eV. The presence of 917.85 eV also confirmed the presence of Ce^{4+} ions. From Raman studies it follows that in Ce-doped ZnO the nonpolar interaction becomes strong and has a dominant intensity, which confirms the high crystal quality.

Acknowledgment. The authors owe sincere thanks to UGC DAE Indore for carrying out XPS and Raman measurements.

REFERENCES

1. M. A. Reshchikov, H. Morkoc, B. Nemeth, J. Nause, J. Xie, B. Hertog, A. Osinsky, *Phys. B*, **401-402**, 358–361 (2007).
2. Seung Soo Lee, Wensi Song, Minjung Cho, Hema L. Puppala, Phuc Nguyen, Huiguang Zhu, Laura Segatori, Vicki L. Colvin, *ACS Nano*, **7**, No. 11, 9693–9703 (2013).
3. C. Karunakaran, P. Gomathisankar, G. Manikandan, *Chem. Phys*., **123**, 585–594 (2010).
4. Jinghai Yang, Ming Gao, Lili Yang, Yongjun Zhang, Jihui Lang, Dandan Wang, Yaxin Wang Huilian Liu, Hougang Fan, *Appl. Surf. Sci*., **255**, 2646–2650 (2008).
5. Wai Kian Tan, Khairunisak Abdul Razak, Zainovia Lockman, Go Kawamura, Hiroyuki Muto, Atsunori Matsuda, *Opt. Mater*., **35**, 1992–1907 (2013).
6. J. Iqbal, X. Liu, H. Zhu, Z.B. Wu, Y. Zhang, D. Yu, R. Yu, *Acta Mater*., **57**, 4790–4796 (2009).
7. G. Srinivasan, R. T. Rajendra Kumar, J. Kumar, *Sol-Gel Sci. Technol*., **43**, 171–177 (2007).
8. Achamma George, Suchinder K. Sharma, Santa Chawla M. M. Malik, M. S. Qureshi, *J. Alloys Compd*., **509**, 5942 (2011).
9. E. Beche, P. Charvin, D. Perarnau, S. Abanades, G. Flamant, *Surf. Interface Anal*., **40**, 264–267 (2008).
10. A. Arguello, D. L. Rousseau, S. P. S. Porto, *Phys. Rev*., **181**, 1351–1363 (1969).
11. M. L. Glasser, *J. Phys. Chem. Solids*, **10**, 229–241 (1959).
12. Jihui Lang, Qiang Han, Jinghai Yang, Changsheng Li, Xue Li, Lili Yang,Yongjun Zhang, Ming Gao, Dandan Wang, Jian Cao, *J. Appl. Phys*., **107**, 074302(1–4) (2010).